PolSAR Mosaic Normalization for Improved Land-Cover Mapping

Oleg Antropov, *Student Member, IEEE*, Yrjö Rauste, Anne Lönnqvist, and Tuomas Häme

***Abstract*—This letter describes an algorithm development for the production of a large-scale fully polarimetric synthetic aperture radar (SAR) (PolSAR) mosaic using multitemporal Advanced Land Observing Satellite Phased Array type L-band SAR acquisitions. The PolSAR data were collected during the snow-melting season in 2007 over Finnish Lapland, resulting in considerable radiometric differences between mosaiced scenes originating at different dates. Several variants of polarimetric seam hiding between the original PolSAR images were proposed and evaluated in order to effectively eliminate stripes in the mosaic. The impact of such seam-hiding procedure on PolSAR classification performance was studied, along with the technical aspects of producing the PolSAR mosaic. The obtained results indicate the advantages of the considered seam-hiding procedures for producing homogeneous mosaics and obtaining consistent classification results in a single classification step.**

***Index Terms*—Classification, forestry, land cover, polarimetry, synthetic aperture radar (SAR).**

I. Introduction

THE modern generation of spaceborne synthetic aperture radar (SAR) sensors offers possibilities for global environmental monitoring and land-cover mapping at high-resolution scale using multipolarization data. Obviously, the ability to combine fully polarimetric SAR (PolSAR) scenes into homogeneous mosaics, analogically to single- and dual-polarization SAR data [1]–[3], would boost the applicability and effectiveness of PolSAR mapping techniques. It is of particular interest in situations when it appears hard to find adequate reference data for each individual PolSAR image. However, the current availability of PolSAR data (e.g., time intervals between the acquisitions of neighboring scenes), as well as its sensitivity to environmental factors, puts some limitations on the production and further use of such mosaics. Thus, it is important to see how multitemporal PolSAR data acquisitions influence mosaic classification accuracy and to identify techniques that are suitable for the processing of such multipolarization data. Other important issues include the identification of application areas where such mosaics of multidate PolSAR images can be effectively used, as well as pinpointing possible challenges and drawbacks of such a combined PolSAR product.

Manuscript received July 19, 2011; revised February 17, 2012; accepted March 1, 2012. This work was supported in part by the Finnish Academy through the CarbBal project, by the RECOVER project of the Framework Program 7 of the European Commission, and in part by the VTT Graduate program.

The authors are with the Remote Sensing Group, VTT Technical Research Centre of Finland, 02044 Espoo, Finland (e-mail: oleg.antropov@vtt.fi).

Color versions of one or more of the figures in this paper are available online at http://ieeexplore.ieee.org.

Digital Object Identifier 10.1109/LGRS.2012.2190263

Land-cover classification challenges in the boreal region are primarily connected with forest-mapping techniques. For forest applications, longer wavelengths are more suitable, particularly at P- and L-bands. In this letter, L-band PolSAR data were used. They were acquired by the Advanced Land Observing Satellite (ALOS) Phased Array type L-band SAR (PALSAR) sensor [4], which provided multipolarization information, well suitable for forest mapping, during its lifetime span of over five years.

The objective of this letter is to evaluate the possibilities of land-cover mapping using a PolSAR mosaic produced from ALOS PALSAR images during the snow-melting season. In particular, the goals include, we believe for the first time, performing seam hiding of PolSAR image produced from spaceborne multitemporal acquisitions and quantitative evaluation of the influence of such procedure on the classification performance of several traditional PolSAR classification techniques. This letter is organized as follows. First, the technical aspects of producing the mosaic are given. Then, several seam-hiding approaches preserving scattering-mechanism (SM) information are proposed, with further evaluation of the impact on PolSAR classification accuracy.

II. Materials and Methods

A. Study Site, PolSAR, and In Situ Data

The study site was chosen at a high-enough latitude to ensure overlap between PolSAR images from the neighboring orbits of the ALOS satellite. The center coordinates of the study site were $68^{\circ}30'$ north, $27^{\circ}30'$ east. The site represents a typical Finnish taiga, with dense and sparse forest covering the majority of the area, with some considerable proportion of open bogs and other peat land. The study area covered the southern part of Lake Inari in the north and the eastern end of the Lokka reservoir in the south.

Polarimetric scenes from two adjacent orbits were used in the mosaic production, with imagery acquired on April 2, 2007 (orbit 6327, the eastern part of the mosaic) and on April 19, 2007 (orbit 6575, the western part). For both acquisition days, the temperature had fluctuated near 0 °C during the previous days, with a clear sky before the image acquisition. The snow-cover situation was characterized by processes of transition from dry to wet state. All the scenes were fully polarimetric with an incidence angle of 24°. These polarimetric products have a pixel spacing of about 3.5 m along track (azimuth) and 9.4 m cross track (slant range). The image swath width was 29.3 km.

A digital elevation model (DEM) from the National Land Survey of Finland was used for image orthorectification. This DEM was produced using digitized contour lines of

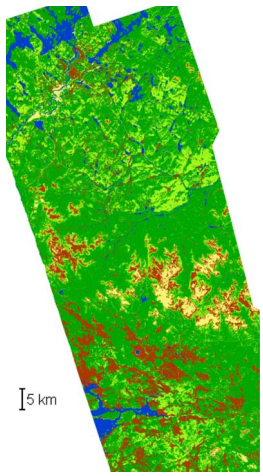

Fig. 1. Reference land-cover/use map. (Blue) Water. (Brown) Peat land. (Light green) Sparse forest. (Dark green) Dense forest. (Yellow) Other. © SYKE.

topographic maps at 1:20 000, with a pixel spacing of 25 m. The vertical accuracy is estimated [5] to be better than 2 m.

The CORINE Land Cover 2000 (CLC) [6] produced by the Finnish Environment Institute (SYKE) was used as ground reference data in the study. The spatial resolution of the land-cover data was 25 m as well. The land-cover map is shown in Fig. 1, with original 17 land-cover classes merged into five major superclasses in this representation, namely, "sparse forest," "dense forest," "peat land," "water," and "other." The latest class represents, in particular, urban and artificial structures, pastures on highlands, and some other composite ecological classes that are hard to describe using polarimetric observables and was masked out before classification.

B. Orthorectification and Geometry Revision

The polarimetric PALSAR products (Level 1.1) included the full scattering matrix. Extracted single-look complex data were subsequently converted to the Stokes matrix format, averaged over six pixels in the along-track direction, and transferred to the coherency matrix format. This procedure resulted in a set of images with a pixel spacing of 21 m in azimuth and approximately 21 m in ground range.

Furthermore, all the data were resampled independently using bilinear interpolation with in-house orthorectification program [7]. A radiometric normalization was performed to eliminate radiometric variation due to terrain elevation variation. The power of each pixel was normalized with respect to the projected area of the scattering element, analogously to description given, e.g., in [8]. The projection was made to a plane perpendicular to the propagation direction of the incoming radar pulse. This form of radiometric normalization eliminates the topographic effects on received power in terrain types whose radar cross section per unit of projected area is independent of the incidence angle.

In order to avoid geometric errors and to supplement the available ALOS image geometry information, manually measured ground control points (GCPs) and automatically measured tie points were used to revise image geometry. The GCPs were measured in the down-averaged PALSAR scenes and map data from the map service of the National Land Survey of Finland. The tie-point and GCP observations were submitted to a block adjustment procedure [1], where three geometry-revision parameters were determined for each scene: translation in northing, translation in easting, and rotation. These parameters were solved using least squares adjustment, which minimizes approximation error over the whole set of observations. The initial geometry information in orthorectification was based on the equations presented in [9].

C. Considerations on Polarimetric Seam Hiding

In the context of the herein described polarimetric mosaic production, we can identify several possible methods for further reduction of radiometric differences between the acquired PolSAR scenes. Obviously, it is not possible to correct for the change in SMs that actually took place because of the seasonal changes (snow melting). However, eliminating the radiometric difference between neighboring stripes (called "normalization" further in this letter) has proved to be an important image-processing step capable of improving further classification results [2].

Such a normalization technique could be implemented, e.g., for each component of the polarimetric coherency (or covariance) matrix. This would, however, result in an unpredictable change of SMs after normalization, if the correction coefficients were different for different components of the coherency matrix.

Another option is the use of the span of the covariance matrix [or total backscattered power (TP)] in order to calculate the corrective gain. Afterward, a pixel-by-pixel multiplication of the whole covariance matrix $\mathbf{C}_{ij}$ by the obtained corrective gain can be performed, ensuring the preservation of SMs for each processed pixel [11]. Technically, the approach follows the method suggested for balancing the intensity between neighboring strips of single-polarization SAR imagery [2] but uses the values of TP instead. In this letter, only two neighboring orbits were available, and scenes acquired on the right orbit are corrected with respect to the left-orbit scenes. The correction procedure simplifies to calculating normalization ratio $B_{rl} = \langle P^l_{\text{total}} \rangle / \langle P^r_{\text{total}} \rangle$, where P^i_{total} is the respective TP for the ith orbit and denotes spatial averaging over a certain area. New covariance matrix values for the right-orbit scenes are obtained as $\hat{\mathbf{C}}^R_{ij} = B * \mathbf{C}^R_{ij}$. This approach preserves polarimetric relations and modifies only the respective TP values. As TP is an important feature characterizing a pixel [12], it is of interest to see how the proposed seam-hiding procedure affects classification for land-cover-mapping purposes.

Then, possible normalization methods, further evaluated in this study, include the PolSAR mosaic correction using the normalization ratio B_{rl} calculated as follows: ***Method 1)*** at the whole extent of the mosaiced scenes, ***Method 2)*** using only pixels from the overlapping areas between the mosaiced scenes, and ***Method 3)*** using only those pixels from the overlapping areas, where a dominating SM is preserved [13]. This ensures that pixels that significantly changed their backscattering signature are excluded from calculation. The corresponding powers of the SMs can be provided by incoherent PolSAR decompositions, considering the primarily natural-media composition of the imaged area.

D. PolSAR Analysis Methods and Software

Three-Component Decomposition: Under the reciprocity assumption, Freeman and Durden [14] suggested a simple three-component model for the decomposition of the covariance matrix, implying complete decorrelation between the copolarized and cross-polarized scattering terms. The model provides information about scattering contributions from several types of canonical targets, described by double-bounce, surface, and volume SMs. One of the most well-known problems associated with this decomposition is the possibility of obtaining negative power estimates of the surface or double-bounce contribution. Therefore, some regularization is needed to assure the physical consistency of the decomposition [15]. With this idea in mind, we have used several modified decompositions along with the traditional one, as presented in [16]–[18], augmented by regularization [15] for those pixels, where negative powers were still obtained.

Entropy–Alpha–Anisotropy Analysis: A popular unsupervised target-classification method is based on the eigendecomposition of the polarimetric coherence matrix [19], [20]. It uses such polarimetric characteristics for the description of target properties as entropy and the averaged alpha angle. Entropy H covers a dynamic range from zero to one, being a measure of the randomness of the scatterer, from deterministically polarized to isotropically depolarized scatter, respectively. The alpha angle α characterizes, through a unitary transformation, an SM (zero is a sphere symmetry, 45 is a dipole, and 90 is a dihedral or helix) independently from a rotation of the measurement coordinates. The mentioned model was further augmented by the anisotropy measure $A \in [0; 1]$ to distinguish between different classes with similar cluster centers, differentiating between single- and multiple-target returns.

The categorized map of the alpha angle against entropy provides an initial classification of PolSAR imagery, after which anisotropy can be used for further analysis. More advanced semisupervised approaches [21], [22] use maximum-likelihood (ML) classification, initially seeded by the $H/A/\alpha$ classes and further iterated by the complex Wishart distribution of the coherency matrix. The complex Wishart algorithm is generally an ML estimator, assigning each sample coherency matrix to one of the associated classes on the basis of the minimum Wishart matrix distance. Further manual labeling of the obtained segments is performed to produce a land-cover/use map.

Supervised Classification Using Wishart Classifier: In supervised classification, training areas are defined manually for each class from the Pauli color-coded presentation or reference ground plot data. Then, the classifier calculates the Wishart statistics of the training areas and assigns each pixel to the closest class using the ML decision rule. The accuracy of the classification is further evaluated against the CLC data. An interface provided by the European Space Agency PolSARpro software [9] was used for supervised Wishart classification.

III. Experimental Data Analysis

A total of 77 tie-point observations were measured using automatic image correlation. A set of GCPs was measured in all four scenes. After the elimination of gross errors, 13 GCPs were used in block adjustment [1]. The residual rmses of the tie points were 8.9 m in northing and 9.5 m in easting. The rmses of the GCP observation were 13.6 m in northing and 19.8 m in easting. The obtained polarimetric mosaic in Pauli color-coded representation is shown in Fig. 2(a) and (b). Here, we used two different ways to combine orthorectified images, favoring the near- or far-range parts of the original PolSAR images. This was done in order to additionally evaluate the influence of near- to far-range choice on the classification accuracy performance of the mosaic.

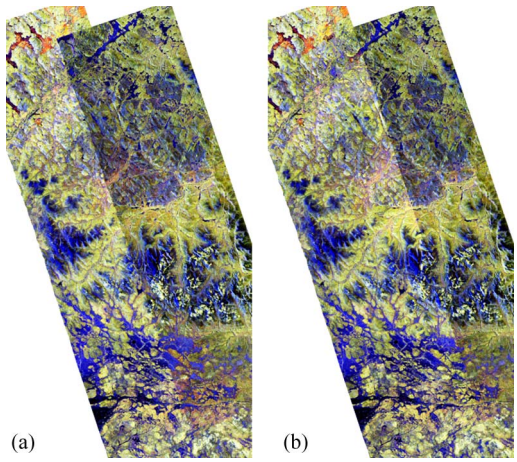

Fig. 2. Pauli color-coded representations of the PolSAR mosaic without seam hiding. (a) Near-range data on top. (b) Far-range data on top. HH–VV is depicted in red, HV is depicted in green, and HH+VV is depicted in blue. © JAXA and METI 2007.

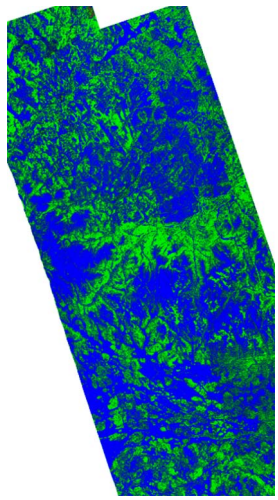

Fig. 3. Color-coded composite of the PolSAR mosaic. (Red) Double-bounce, (green) volume, and (blue) surface scattering contributions to TP.

Dominating SMs were identified using the three-component decomposition (Fig. 3) and a simple rule-based approach, with some SM considered dominant if its power accounts for more than 50% of the TP in an analyzed resolution cell. The mixed category of pixels appeared to be relatively insignificant (0.71% of the total amount of pixels) and was not used in computing the normalization ratio. The implemented approaches allowed obtaining visibly more homogeneous PolSAR data representations when compared to the initial noncorrected mosaic. One of the examples is shown in Figs. 4 and 5, illustrating the difference between the original and normalized PolSAR mosaics.

It is interesting to note that the use of the different model-based decompositions [16]–[18] had practically no influence on the pixels' assigned dominating SM (the observed deviation

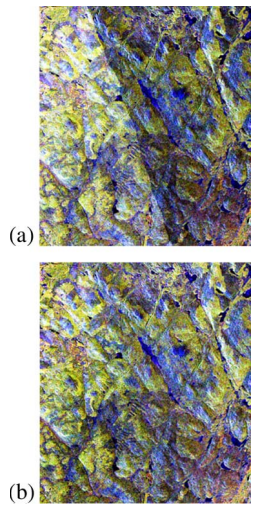

Fig. 4. Enlarged fragments of the mosaic, size 20 km × 17.5 km. (a) Original. (b) Normalized. Color legend follows Fig. 2. © JAXA and METI 2007.

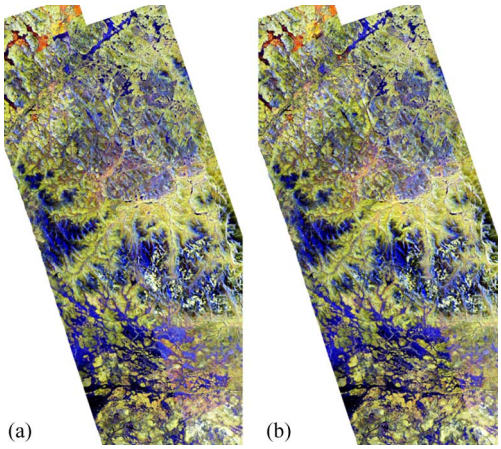

Fig. 5. Pauli color-coded representation of the PolSAR mosaic after the seam-hiding procedure; the normalization strategy after Method 3 is used. (a) Near-range data on top. (b) Far-range data on top. HH–VV is depicted in red, HV is depicted in green, and HH+VV is depicted in blue. © JAXA and METI 2007.

was less than 2%). It can be explained by the simplicity of the adopted decision rule and the composition of the land-cover classes in the scene, mostly characterized by a mixture of volume and surface scattering. Majority of the pixels in the overlapping areas were found to preserve their dominant SM, despite, e.g., the actual change in snow wetness. The use of TP with the preservation of the dominating SM allowed excluding pixels demonstrating a strong seasonal change (e.g., jammed ice in the north of the mosaic transferring to open-water areas). Some residual imbalance in the southeastern scene can be explained by the influence of the relatively mountainous area in the overlapping area between the left- and right-orbit scenes.

Classification results for both combinations of the polarimetric mosaic along with corresponding normalized versions are collected in Table I, both for multiclass and forest–nonforest classifications. Three polarimetric seam-hiding approaches were used to correct the mosaic (see Section II-C).

In supervised Wishart classification, a total of 24 training sets covering the whole area of the mosaic were used, representing about 14 000 out of more than 8 million available pixels. As expected, the supervised Wishart classification has provided

TABLE I
POLSAR MOSAIC LAND-COVER CLASSIFICATION. THE OVERALL ACCURACY ESTIMATES ARE GIVEN BOTH FOR MULTI CLASS AND FOREST NONFOREST (IN BRACKETS) CLASSIFICATIONS

	Original	*Method 1*	*Method 2*	*Method 3*
Mosaic 1, Fig. 2 a				
Target decomposition + Wishart + labeling	61.4% (79.2%)	63.3% (81.0%)	63.9% (82.1%)	64.6% (83.4%)
Supervised Wishart	63.1% (81.4%)	65.1% (83.7%)	65.6% (84.5%)	66.7% (85.9%)
Mosaic 2, Fig. 2 b				
Target decomposition + Wishart + labeling	64.4% (83.0%)	65.6% (84.2%)	65.9% (84.4%)	67.2% (86.1%)
Supervised Wishart	66.4 % (85.1%)	68.1% (87.0%)	67.7% (86.4%)	69.5% (88.8%)

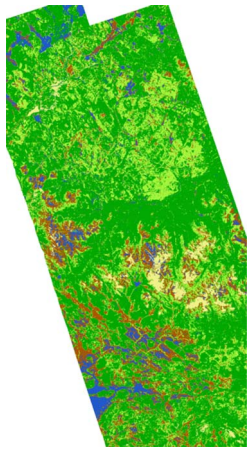

Fig. 6. Result of supervised classification from the PolSAR mosaic shown in Fig. 5(b). Color legend follows Fig. 1.

better classification results, though the difference appeared to be not very significant compared to the unsupervised approach and generally heavily dependent on the choice of training data. The obtained results emphasize an important role of the total power in PolSAR data classification, often neglected when using pure target model-based decompositions, as well as some statistical classification approaches utilizing selected polarimetric features. The application of the proposed polarimetric seam hiding allowed increasing classification accuracy by some 2.8%–3.6%, with the best results obtained for the PolSAR mosaic normalization strategy employing *Method 3*, Section II-C. While these results need further validation in different natural or seminatural environments, they provide a good insight into what can be expected from the suggested polarimetric seam-hiding approaches.

As for the relatively low overall classification accuracy, it can be considered the best one attainable under the given seasonal conditions taking into account the multitemporal nature of the mosaic, as well as the original nature of the reference data. Moreover, it is generally difficult to associate available ecological classes to the obtained radar target classifier [23]. For example, the difference in the definition of sparse and dense forests is quite technical (the percentage of canopy cover and tree height thresholds) and can be hard to capture adequately by radar. The kappa coefficients of agreement [24] were from fair to moderate in all the performed classifications. Some additional gain in accuracy was achieved when a straightforward water detection based on TP was utilized, as, e.g., in [25]. It

particularly allowed circumventing the confusion between peat land and watered areas observed in Figs. 1 and 6.

It is also interesting to note the difference in the classification performance of the two versions of the mosaic. In overlapping areas, mostly densely and sparsely forested areas were dominating, and the far-range PolSAR data demonstrated a slightly higher sensitivity to the presence of vegetation than the near-range PolSAR data. For the near-range data, the observed higher confusion between forested and open areas is explained by the steeper incidence angle and generally high penetration through canopy at L-band. It resulted in obtaining higher accuracies for the given land-cover composition when far-range areas were used in the mosaic compilation.

IV. Conclusion

A multidate PolSAR mosaic has been produced from PolSAR imagery acquired from two adjacent orbits in such a way that any polarimetric analysis or classification can be performed on it in a single step. The classification accuracy of several classification approaches has been evaluated using the produced PolSAR mosaic, with both supervised and unsupervised approaches giving moderate results, with a better performance when far-range SAR data were given preference in the production of the mosaic. Suggestions on the improvement of the classification performance have been made in order to hinder the effects of the multitemporal nature of the PolSAR mosaic. Several methods for polarimetric seam hiding (normalization) have been proposed and implemented, resulting in the improvement of the overall classification accuracy performance. These methods are based on eliminating differences in the total backscattered power between the overall neighboring scenes or their selected areas. They preserve the SMs due to the use of the span of the polarimetric coherency (or covariance) matrix and emphasize the importance of the total backscattered power in land-cover/use classification employing PolSAR imagery. We expect the demonstrated seam-hiding techniques to be most applicable over forested terrain, with PolSAR data acquired preferably during summer (or dry) season.

Acknowledgment

The ALOS/PALSAR data (acquired by the Japanese Aerospace Exploration Agency) were provided by the European Space Agency in the context of ALOS/Aden announcement of opportunities project AOALO.3713. The authors would like to thank the anonymous reviewers for discussions and valuable suggestions on the manuscript.

References

[1] G. De Grandi, P. Mayaux, Y. Rauste, A. Rosenqvist, M. Simard, and S. S. Saatchi, "The global rain forest mapping project JERS-1 radar mosaic of tropical Africa: Development and product characterization aspects," *IEEE Trans. Geosci. Remote Sens.*, vol. 38, no. 5, pp. 2218–2233, Sep. 2000.

[2] M. Shimada and T. Ohtaki, "Generating large-scale high-quality SAR mosaic datasets: Application to PALSAR data for global monitoring," *IEEE J. Sel. Topics Appl. Earth Obs. Remote Sens.*, vol. 3, no. 4, pp. 637–656, Dec. 2010.

[3] G. D. De Grandi, A. Bouvet, R. M. Lucas, M. Shimada, S. Monaco, and A. Rosenqvist, "The K&C PALSAR mosaic of the African continent: Processing issues and first thematic results," *IEEE Trans. Geosci. Remote Sens.*, vol. 49, no. 10, pp. 3593–3610, Oct. 2011.

[4] A. Rosenqvist, M. Shimada, N. Ito, and M. Watanabe, "ALOS PALSAR: A pathfinder mission for global-scale monitoring of the environment," *IEEE Trans. Geosci. Remote Sens.*, vol. 45, no. 11, pp. 3307–3316, Nov. 2007.

[5] Y. Rauste, "Techniques for wide-area mapping of forest biomass using radar data," Ph.D. Thesis, VTT Publications, Espoo, Finland, 2005, vol. 591.

[6] P. Härmä, R. Teiniranta, M. Törmä, R. Repo, E. Järvenpää, and M. Kallio, "Production of CORINE2000 land cover data using calibrated LANDSAT 7 ETM satellite image mosaics and digital maps in Finland," in *Proc. Int. Geosci. Remote Sens. Symp.*, Sep. 2004, vol. 4, pp. 2703–2706.

[7] Y. Rauste, A. Lönnqvist, M. Molinier, J.-B. Henry, and T. Häme, "Orthorectification and terrain correction of polarimetric SAR data applied in the ALOS/Palsar context," in *Proc. Int. Geosci. Remote Sens. Symp.*, 2007, pp. 1618–1621.

[8] D. Small, "Flattening gamma: Radiometric terrain correction for SAR imagery," *IEEE Trans. Geosci. Remote Sens.*, vol. 49, no. 8, pp. 3081–3093, Aug. 2011.

[9] J. C. Curlander, "Location of spaceborne SAR imagery," *IEEE Trans. Geosci. Remote Sens.*, vol. GE-20, no. 3, pp. 359–364, Jul. 1982.

[10] E. Pottier, L. Ferro-Famil, S. Allain, S. Cloude, I. Hajnsek, K. Papathanassiou, A. Moreira, M. Williams, A. Minchella, M. Lavalle, and Y.-L. Desnos, "Overview of the PolSARpro v4.0 Software. The open source toolbox for polarimetric and interferometric polarimetric SAR data processing," in *Proc. Int. Geosci. Remote Sens. Symp*, 2009, pp. IV-936–IV-939.

[11] J.-S. Lee, M. R. Grunes, and G. de Grandi, "Polarimetric SAR speckle filtering and its implication for classification," *IEEE Trans. Geosci. Remote Sens.*, vol. 37, no. 5, pp. 2363–2373, Sep. 1999.

[12] F. Cao, W. Hong, Y. Wu, and E. Pottier, "An unsupervised segmentation with an adaptive number of clusters using the SPAN/ H/ α/ A space and the complex Wishart clustering for fully polarimetric SAR data analysis," *IEEE Trans. Geosci. Remote Sens.*, vol. 45, no. 11, pp. 3454–3467, Nov. 2007.

[13] J. S. Lee, M. R. Grunes, E. Pottier, and L. Ferro-Famil, "Unsupervised terrain classification preserving polarimetric scattering characteristics," *IEEE Trans. Geosci. Remote Sens.*, vol. 42, no. 4, pp. 722–731, Apr. 2004.

[14] A. Freeman and S. L. Durden, "A three-component scattering model for polarimetric SAR data," *IEEE Trans. Geosci. Remote Sens.*, vol. 36, no. 3, pp. 963–973, May 1998.

[15] J. J. Van Zyl, Y. Kim, and M. Arii, "Requirements for model based decompositions," in *Proc. Int. Geosci. Remote Sens. Symp.*, 2008, pp. V-417–V-420.

[16] Y. Yamaguchi, T. Moriyama, M. Ishido, and H. Yamada, "Four-component scattering model for polarimetric SAR image decomposition," *IEEE Trans. Geosci. Remote Sens.*, vol. 43, no. 8, pp. 1699–1706, Aug. 2005.

[17] I. Hajnsek, T. Jagdhuber, H. Schon, and K. P. Papathanassiou, "Potential of estimating soil moisture under vegetation cover by means of PolSAR," *IEEE Trans. Geosci. Remote Sens.*, vol. 47, no. 2, pp. 442–454, Feb. 2009.

[18] O. Antropov, Y. Rauste, and T. Häme, "Volume scattering modeling in PolSAR decompositions: Study of ALOS PALSAR data over boreal forest," *IEEE Trans. Geosci. Remote Sens.*, vol. 49, no. 10, pp. 3838–3848, Oct. 2011.

[19] S. R. Cloude and E. Pottier, "A review of target decomposition theorems in radar polarimetry," *IEEE Trans. Geosci. Remote Sens.*, vol. 34, no. 2, pp. 498–518, Mar. 1996.

[20] S. R. Cloude and E. Pottier, "An entropy based classification scheme for land applications of polarimetric SAR," *IEEE Trans. Geosci. Remote Sens.*, vol. 35, no. 1, pp. 68–78, Jan. 1997.

[21] J.-S. Lee, M. R. Grünes, T. L. Ainsworth, L.-J. Du, D. L. Schuler, and S. R. Cloude, "Unsupervised classification using polarimetric decomposition and the complex Wishart classifier," *IEEE Trans. Geosci. Remote Sens.*, vol. 37, no. 5, pp. 2249–2258, Sep. 1999.

[22] L. Ferro-Famil, E. Pottier, and J.-S. Lee, "Unsupervised classification of multifrequency and fully polarimetric SAR images based on the H/ A/Alpha-Wishart classifier," *IEEE Trans. Geosci. Remote Sens.*, vol. 39, no. 11, pp. 2332–2342, Nov. 2001.

[23] P. Lumsdon, S. R. Cloude, and G. Wright, "Polarimetric classification of land cover for Glen Affric radar project," *Proc. Inst. Elect. Eng.—Radar, Sonar Navig.*, vol. 152, no. 6, pp. 404–412, Dec. 2005.

[24] R. G. Congalton, "A review of assessing the accuracy of classifications of remotely sensed data," *Remote Sens. Environ.*, vol. 37, no. 1, pp. 35–46, Jul. 1991.

[25] P. Mishra, D. Singh, and Y. Yamaguchi, "Land cover classification of PALSAR images by knowledge based decision tree classifiers based on SAR observables," *Progr. Electromag. Res. B*, vol. 30, pp. 47–70, 2011.